J. Fluid Mech. (1998), *vol.* 355, *pp.* 359–381. Printed in the United Kingdom

© 1998 Cambridge University Press

The long-time behaviour of incompressible swept-wing boundary layers subject to impulsive forcing

By M. J. TAYLOR AND N. PEAKE
Department of Applied Mathematics and Theoretical Physics, University of Cambridge,
Silver Street, Cambridge CB3 9EW, UK

(Received 27 May 1997 and in revised form 26 September 1997)

The long-time limit of the response of incompressible three-dimensional boundary layer flows on infinite swept wedges and infinite swept wings to impulsive forcing is examined using causal linear stability theory. Following the discovery by Lingwood (1995) of the presence of absolute instabilities caused by pinch points occurring in the radial direction in the boundary layer flow of a rotating disk, we search for pinch points in the crossflow direction for both the model Falkner–Skan–Cooke profile of a swept wedge and for a genuine swept-wing configuration. It is shown in both cases that, within a particular range of the parameter space, the boundary layer does indeed support pinch points in the wavenumber plane corresponding to the crossflow direction. These crossflow-induced pinch points do not constitute an absolute instability, as there is no simultaneous pinch occurring in the streamwise wavenumber plane, but nevertheless we show here how they can be used to find the maximum local growth rate contained in a wavepacket travelling in any given direction. Lingwood (1997) also found pinch points in the chordwise wavenumber plane in the boundary layer of the leading-edge region of a swept wing (i.e. at very high flow angles). The results presented in this paper, however, demonstrate the presence of pinch points for a much larger range of flow angles and pressure gradients than was found by Lingwood, and indeed describe the flow over a much greater, and practically significant, portion of the wing.

1. Introduction

An understanding of the stability properties of the boundary layers on swept wings is essential for the development of laminar-flow technology on the next generation of civil aircraft. Laminar flow control is concerned with the delay of laminar–turbulent transition on the wing using either passive means (e.g. modification of pressure gradient, wall shaping) or active means (e.g. wall suction, heat transfer), in order to ensure an extensive region of low-skin-friction drag over much of the surface of the wing, thereby improving fuel efficiency and reducing aircraft operating costs. Linear stability theory together with empirical transition prediction methods (Van Ingen 1956) have been used extensively in the design of swept aircraft wings. These methods use the concept that a small disturbance introduced into the boundary layer will trigger transition when it has been amplified by a factor of e^N. The flow is modelled as being convectively unstable, so the boundary layer can remain laminar until the disturbance has travelled sufficiently far downstream to have grown to a large enough amplitude to cause nonlinearities that trigger transition. The e^N

method is based on tracking single normal modes in the boundary layer using various integration strategies, such as the the envelope method (Malik & Orszag 1980), and does not model the full physics of the instability waves in the boundary layer flow. It does, however, provide a means for correlation of transition location using linear stability theory with experiment and flight tests. In this paper we will describe an alternative method, in which the long-time limit of the response of the boundary layer is evaluated by investigating the presence of crossflow-induced pinch points between modes in the crossflow–wavenumber plane. We will demonstrate how this property can be used to follow the evolution of a wavepacket, and in particular to determine the maximum growth rate for propagation in a given direction, with the significant advantage of being able to study the range of unstable frequencies contained in the wavepacket, rather than just unstable modes of a single frequency as performed in an e^N calculation.

The work of Briggs (1964) and Bers (1975) in plasma physics has shown that in two dimensions an absolute instability is caused by modes propagating in opposite directions pinching together so that the group velocity component in the corresponding physical direction is zero. A flow that is absolutely unstable supports disturbances that grow in time at a fixed point in space, eventually leading to nonlinearities and thereby causing transition to turbulence, and absolute instability mechanisms have been demonstrated to exist for a number of flow regimes: for near-wake flows (Betchov & Criminale 1966; Koch 1985), for flows over a compliant surface (Brazier-Smith & Scott 1984), and for mixing layers with backflow (Huerre & Monkewitz 1985). These authors have shown that variation of a control parameter, such as the Reynolds number, can cause pinch points to occur, leading to local absolute instabilities. In three dimensions Brevdo (1991) has shown that pinch points occurring in both spatial complex wavenumber planes simultaneously are necessary (and sufficient) for absolute instability. Lingwood (1997) found that the flow near the attachment line of a swept wing supports pinch points in the complex wavenumber plane corresponding to the chordwise direction only, but it is emphasised that no simultaneous spanwise pinch points were found, indicating the absence of an absolute instability mechanism for this flow.

Lingwood (1995) has demonstrated that within a certain range of the parameter space, the boundary layer flow over a disk rotating in an otherwise still fluid supports absolute instabilities caused by the occurrence of a pinch point in the radial direction. (The simultaneous occurrence of a pinch point in the azimuthal plane is not necessary for absolute instability in this case only, since the circular symmetry forces the azimuthal wavenumber to be an integer.) The experimental analysis of Lingwood (1996) demonstrated that the onset of laminar–turbulent transition on the rotating-disk boundary layer is indeed consistent with the characteristics of an absolutely unstable flow. The flow over the rotating disk is characterized by the presence of a velocity component which is inflectional in the radial direction, and since this is also a feature of the crossflow velocity component in the three-dimensional boundary layer on a swept wing, M. Gaster (1994, personal communication) suggested that pinch points may also be supported by the swept-wing boundary layer. It was precisely this suggestion which was investigated by Lingwood (1997), and as mentioned above pinches were indeed found at high flow angles close to the leading edge (actually in the wing chordwise direction, which for high flow angle is close to the crossflow direction). In this paper we conduct a more extensive search of parameter space, and locate another pinch, this time in the genuine cross-stream direction, which exists for a much larger range of flow angles and at lower Reynolds numbers than was found by Lingwood, and which is therefore capable of describing the flow over a considerably larger portion of the wing.

A considerable body of experimental and theoretical work already exists on swept-wing transition, and only a brief summary is necessary here. Gray (1952) observed in experiments that transition to turbulence occurs at a much lower Reynolds number on swept wings than on unswept wings, and that the boundary layer flow over the swept wing is characterized by the appearance of striations in the laminar boundary layer, caused by a series of stationary vortices with axes lying in the streamwise direction due to the inviscid instability of the inflectional crossflow velocity component (Gregory, Stuart & Walker 1955). Travelling crossflow instabilities have also been observed in experiments on a swept cylinder by Poll (1985). Disturbances in the boundary layer are generally amplified by the inviscid crossflow mechanism in the negative pressure rise region near the leading edge of the wing, and by the viscous streamwise Tollmien–Schlichting (TS) mechanism in the flat pressure region at the mid-chord of the wing. These disturbances initially grow linearly, while travelling downstream, until they amplify sufficiently to enter a region where nonlinear interactions and the development of secondary instabilities cause the breakdown of the laminar flow into turbulence (Malik, Li & Chang 1994). The triggering of transition on a swept-wing boundary layer can also be caused by the instability of the attachment-line boundary layer to TS waves, which can be stabilized using suction (Hall, Malik & Poll 1984). The analysis in this paper is, of course, relevant to just the linear stages of swept-wing boundary layer instabilities.

In this paper we will first investigate the presence of crossflow-induced pinch points in the Falkner–Skan–Cooke boundary layer. This family of profiles describes the boundary layer on a swept wedge, and is often used to model the boundary layer on a swept wing, since it allows the magnitude of the inflectional crossflow component to be varied in a systematic way. In this respect we will vary both the Hartree pressure gradient parameter and the flow angle in order to investigate the effect of changes in the crossflow component on the pinch point mechanism, and also look at the effect of suction and blowing. The boundary layer is assumed to be laminar with no leading-edge contamination, and we will also assume that the velocity profiles have not been modified by the presence of large convective disturbances, e.g. travelling and stationary crossflow vortices, that have not yet triggered transition in the boundary layer. In §2 we describe the theory and methods used to perform the analysis, and in §3 results are presented for the Falkner–Skan–Cooke boundary layer. In §4 we then go on to study the pinch point mechanism on a NASA laminar flow airfoil, in order to demonstrate that the mechanism is indeed supported by a physical swept wing. We then analyse these results in §5 and give our conclusions in §6.

2. Problem formulation

2.1. *Mean flow*

The Falkner–Skan–Cooke (FSC) solution for the incompressible boundary layer flow over an infinite swept wedge at zero angle of attack is described by Cooke (1950) and will be used here to provide a model of the boundary layer flow over a swept wing. Although the pressure gradient on a genuine airfoil is not constant over the chordlength, which is an assumption of the FSC solution, there are two parameters in the FSC formulation that allow the magnitude of the crossflow to be varied, and which enable us to study in a systematic way the properties of a boundary layer

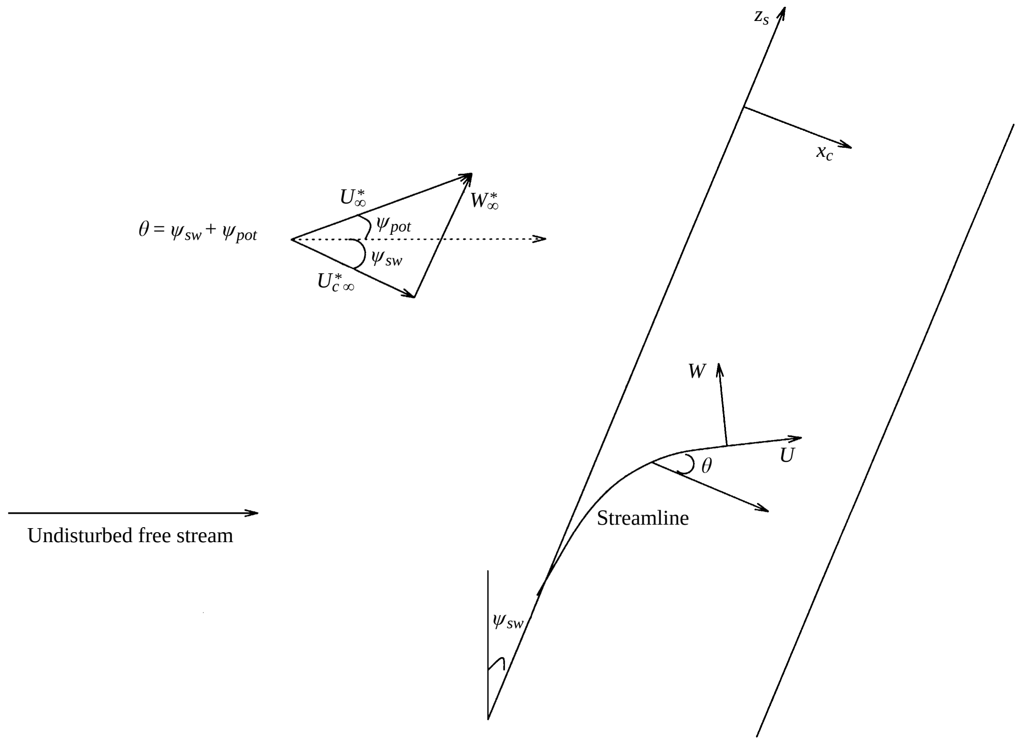

FIGURE 1. The FSC flow geometry, where U and W are the streamwise and crossflow components of the non-dimensionalized velocity respectively. U^*_∞ is the speed of the local potential flow which is at an angle ψ_{pot} with respect to the undisturbed free stream, with components $U^*_{c\infty}$ and $W^*_{s\infty}$ in the chordwise and spanwise directions respectively.

similar to that found on a swept wing. (In §4 we will analyse the boundary layer on a genuine swept wing.) The first parameter of the FSC formulation is the dimensionless pressure gradient, or 'Hartree', parameter β_H used in the two-dimensional Falkner–Skan boundary layer, and the second is the ratio of spanwise and chordwise velocities. The inviscid free-stream velocity in the chordwise direction normal to the leading edge is taken to be

$$U^*_{c\infty} = C^*(x^*_c)^m,$$

where x^*_c is the chordwise coordinate, C^* is a positive constant and the asterisk denotes dimensional quantities. In the direction parallel to the leading edge the spanwise potential velocity is taken to have the constant value $W^*_{s\infty}$. The wedge angle is $\beta_H\pi/2$, where $\beta_H = 2m/(m+1)$. The boundary layer flow in the chordwise and spanwise directions is now written as

$$U_c = U^*_c/U^*_{c\infty} = f'(\eta),$$

$$W_s = W^*_s/W^*_{s\infty} = g(\eta),$$

where

$$\eta = \left[\frac{(m+1)U^*_{c\infty}}{2\nu^* x^*_c}\right]^{1/2} y^*,$$

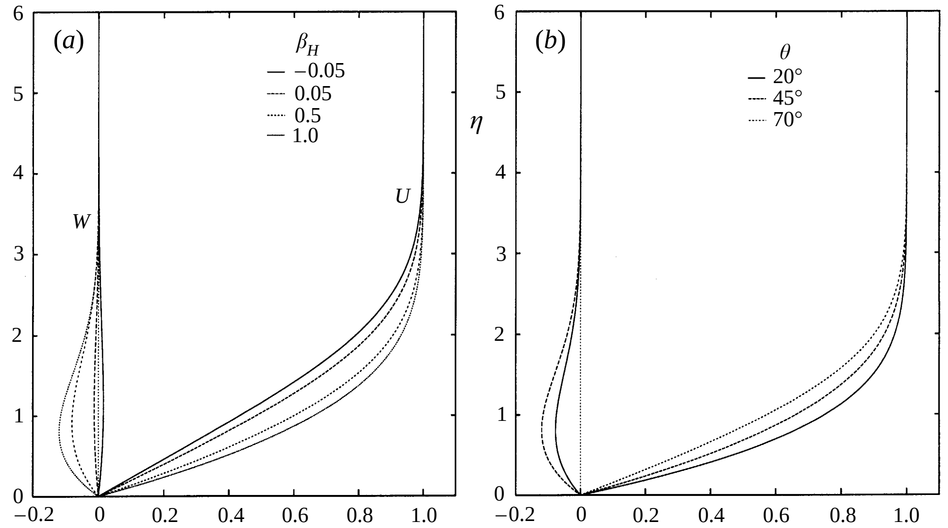

FIGURE 2. (*a*) The FSC velocity profiles for $\beta_H = -0.05,\ 0.05,\ 0.5,\ 1.0$ at $\theta = 45°$. (*b*) The FSC velocity profiles for $\theta = 20°,\ 45°,\ 70°$ at $\beta_H = 1.0$.

y^* is the coordinate in the direction normal to the wedge plane and ν^* is the kinematic viscosity. The functions f and g satisfy

$$f''' + ff'' + \beta_H(1 - f'^2) = 0, \tag{1}$$

$$g'' + fg' = 0, \tag{2}$$

with the boundary conditions

$$f(0) = f'(0) = g(0) = 0, \quad f'(\infty) = g(\infty) = 1. \tag{3}$$

The details of the derivation of this solution are discussed in Rosenhead (1963).

In this paper we will be studying the streamwise and crossflow velocity components, which are constructed using the functions f and g. This is done by choosing the direction of the undisturbed free stream and defining the sweep angle of the wedge, ψ_{sw}, relative to it; see figure 1. The local inviscid outer flow has speed $U^*_\infty = (U^{*2}_{c\infty} + W^{*2}_{s\infty})^{1/2}$, and is in the direction making an angle ψ_{pot} with respect to the undisturbed free stream. The direction of this outer flow defines the streamwise direction, x, and normal to it the crossflow direction, z. The angle between the streamwise direction and the chordwise direction is the flow angle θ, which is now given by

$$\theta = \tan^{-1}\left(\frac{W^*_{s\infty}}{U^*_{c\infty}}\right) = \psi_{sw} + \psi_{pot};$$

see figure 1 for details. Using the local outer velocity U^*_∞ to normalize our flow speeds, it can then be shown that the dimensionless streamwise and crossflow velocity components in the boundary layer are

$$U(\eta) = f'(\eta)\cos^2\theta + g(\eta)\sin^2\theta, \tag{4}$$

$$W(\eta) = (-f'(\eta) + g(\eta))\cos\theta\sin\theta, \tag{5}$$

respectively. In figure 2(*a*) we show the FSC profiles with flow angle $\theta = 45°$, corresponding to maximum crossflow, for a number of pressure gradients. As β_H

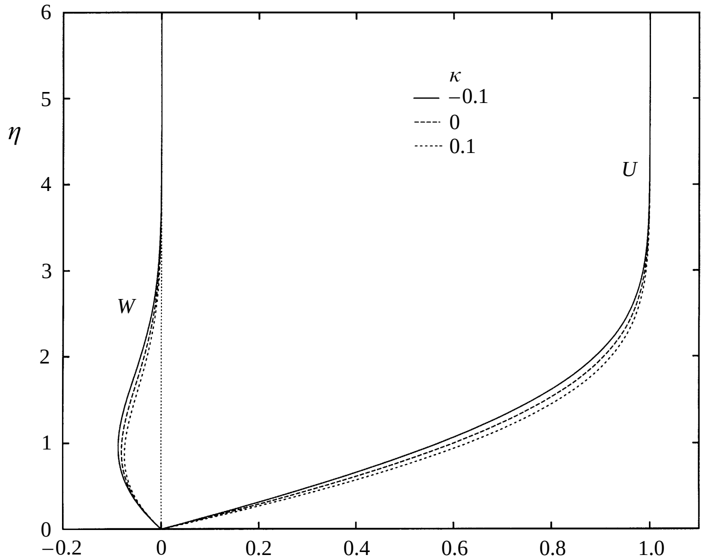

FIGURE 3. FSC velocity profiles for $\beta_H = 0.5$ and $\theta = 45°$ for a range of values of the wall suction/blowing parameter, $\kappa = -0.1, 0, 0.1$.

decreases from 1.0, the inflection point in the crossflow velocity component drifts outwards and the displacement thickness in the streamwise direction increases. In figure 2(*b*) we see that for fixed β_H (in this graph $\beta_H = 1.0$) the crossflow velocity profiles have the same shape, with only the magnitude changing with flow angle. The velocity profiles for the flow angles of 20° and 70° have the same crossflow component, but the streamwise components do differ, with the streamwise displacement thickness increasing as the flow angle increases.

We will also explore the effects of suction and blowing on the stability of the FSC boundary layers by applying the boundary condition

$$f(0) = \kappa,$$

instead of $f(0) = 0$ (Rosenhead 1963). In this way we generate a distribution of suction ($\kappa > 0$) and of blowing ($\kappa < 0$) with wall-normal velocity proportional to $x_c^{*-1/2}$. Figure 3 shows the suction and blowing boundary layer for $\kappa = 0.1, 0$ and -0.1 at $\beta_H = 0.5$ and $\theta = 45°$. The inflection point moves inward/outward and the streamwise displacement thickness decreases/increases with suction/blowing.

2.2. *Linear stability theory*

We use the form of the incompressible linear stability equations discussed by Mack (1984), in which the mean flow is assumed to be parallel so that the problem reduces to finding the eigenvalues of the three-dimensional Orr–Sommerfeld equation. These eigenvalues satisfy the dispersion relation

$$D(\alpha, \beta, \omega, Re) = 0,$$

where α and β are the wavenumbers in the streamwise and crossflow directions respectively, ω is the complex frequency, and Re is the Reynolds number based on the streamwise displacement thickness

$$Re = \frac{U^*_\infty \delta^*}{\nu^*}.$$

At a fixed Reynolds number there are six real quantities in the dispersion relation, namely the real and imaginary parts of α, β and ω, and any two can be determined as eigenvalues when the other four are specified. In order to find the temporal and spatial eigenvalue spectra of the stability problem we use a global boundary-value method (Malik 1990), which gives the higher modes needed for locating pinch points. We use the fourth-order system of equations with two second-order momentum equations and the first-order continuity equation. The differential equations are converted into linear algebraic equations using a finite-difference method on a staggered grid, in order to avoid having to supply an artificial pressure perturbation boundary condition. The eigenvalue spectra are obtained by solving the characteristic determinant of the generalized eigenvalue problem and these global results are then used as guesses for the local eigenvalue solver. The latter uses the shooting method with a fixed-step fourth-order Runge–Kutta integrator, with a Gram–Schmidt orthonormalization procedure at selected integration steps, and a linear Newton–Raphson search procedure (Mack 1984). In this way the higher-order modes can be determined efficiently with good accuracy. Full details of this procedure are given in Taylor (1997).

2.3. *Causal response theory*

We recall that α is the wavenumber in the streamwise direction and β is the wavenumber in the direction of the inflectional profile (i.e. the crossflow direction). We will use the theory of Briggs (1964) to find the causal solution to the impulse response problem in the long-time limit $t \to \infty$. In order to apply Briggs' method we solve the governing equations subject to an impulsive point forcing $\delta(x-x_0)\delta(z-z_0)\delta(t)$, and the space–time evolution of the response is then described by a single-Laplace double-Fourier Green's function of the form

$$G(x,z,t) = \frac{1}{8\pi^3}\int_L \mathrm{d}\omega \int_E \int_F \mathrm{d}\alpha \mathrm{d}\beta \frac{\exp[\mathrm{i}(\alpha(x-x_0)+\beta(z-z_0)-\omega t)]}{D(\alpha,\beta,\omega,Re)}. \tag{6}$$

The inversion contour L in the complex frequency plane is a horizontal line located above all the singularities of the integrand, while the E and F contours are initially taken along the real α- and β-axes respectively. After performing the ω-inversion integral in equation (6), by closing the L contour with semicircles at infinity and using the residue theorem, we find

$$G \sim \frac{H(t)}{4\pi^2 \mathrm{i}}\int_E \int_F \mathrm{d}\alpha \mathrm{d}\beta \sum_{j=1}^{n} \frac{\exp[\psi(\alpha,\beta)t]}{\partial D(\alpha,\beta,\omega_j,Re)/\partial\omega}, \tag{7}$$

where we have considered the discrete response only and neglected the branch cut contributions, which is sufficient to determine the long-time limit of the causal solution (Lingwood 1997). Here

$$\psi(\alpha,\beta) \equiv \psi_r + \mathrm{i}\psi_i = \mathrm{i}\left[\alpha\frac{(x-x_0)}{t} + \beta\frac{(z-z_0)}{t} - \omega(\alpha,\beta)\right], \tag{8}$$

$\omega = \omega_j$ for $j = 1,2,...,n$ are the first-order poles of the ω integrand in equation (6) and $H(t)$ is the Heaviside unit-step function. We use the method of steepest descents to study the asymptotic behaviour of the integral (7) for large t, where $(x-x_0)$ and

$(z - z_0)$ are also large parameters and $u \equiv (x - x_0)/t$ and $v \equiv (z - z_0)/t$ are $O(1)$. We thereby consider the evolution of the boundary layer as measured by an observer moving in the streamwise and crossflow directions with speeds u and v respectively. Dominant contributions are given by the saddle points of $\psi(\alpha, \beta)$, and at these saddle points we have

$$\frac{\partial \omega_r}{\partial \alpha_r} = u, \frac{\partial \omega_r}{\partial \beta_r} = v, \tag{9}$$

$$\frac{\partial \omega_i}{\partial \alpha_r} = 0, \frac{\partial \omega_i}{\partial \beta_r} = 0. \tag{10}$$

At a crossflow-induced pinch point in the β-plane we will have, by definition, $v = 0$ so that

$$\psi_r = (\omega_i - \alpha_i u) = \left(\omega_i - \alpha_i \frac{\partial \omega_r}{\partial \alpha_r}\right).$$

If we now keep $v = 0$ but allow u to vary (as suggested by Lingwood 1997), then the maximum value for ψ_r for varying u occurs when

$$\frac{\partial \psi_r}{\partial u} = \frac{\partial \omega_i}{\partial \alpha_i}\frac{\partial \alpha_i}{\partial u} - \alpha_i - \frac{\partial \alpha_i}{\partial u} u = 0.$$

However, by the Cauchy–Riemann equations

$$\frac{\partial \omega_i}{\partial \alpha_i} = \frac{\partial \omega_r}{\partial \alpha_r} = u,$$

and therefore $\alpha_i = 0$, and hence α is real, at the maximum of ψ_r. By searching for crossflow-induced pinch points we can therefore locate the maximum growth in the streamwise direction using only real values of the streamwise wavenumber α, and this point of maximum growth corresponds to the point where

$$\frac{\partial \omega_i}{\partial \alpha_r} = 0.$$

The crossflow-induced pinch points of the FSC boundary layer and for a genuine swept airfoil are examined in §3 and §4 respectively.

In figure 4 we sketch the contours of positive ψ_r in the (u, v)-plane. The maximum value of ψ_r in this plane occurs when

$$\frac{\partial \psi_r}{\partial u} = \frac{\partial \psi_r}{\partial v} = 0,$$

or equivalently when $\alpha_i = \beta_i = 0$. We have just shown how to calculate the maximum value of ψ_r on the u-axis (i.e. for $v = 0$) by putting $\alpha_i = 0$ and finding the maximum value of ω_i at a β pinch, and this point is marked u^{max} on figure 4. The maximum value of ψ_r in the (u, v)-plane is denoted ψ_r^{max}, and this point is connected to the point u^{max} by a line with $\alpha_i = 0$, as shown in figure 4. In order to find the maximum value of ψ_r in the (u, v)-plane it will be necessary to rotate the axes until the u-axis goes through the point ψ_r^{max}, but we will discuss this further in §5. We also note that if the region enclosed by the zero contour $\psi_r = 0$ contains the origin of the (u, v)-plane, then an absolute instability would occur due to a simultaneous pinch point (with $u = v = 0$) in both wavenumber planes, but no such point was found in our calculations. Further details of this analysis are given in Lingwood (1997).

In order to locate pinch points in the crossflow wavenumber β-plane we therefore keep the value of α, the streamwise wavenumber, real and the E-contour fixed on the

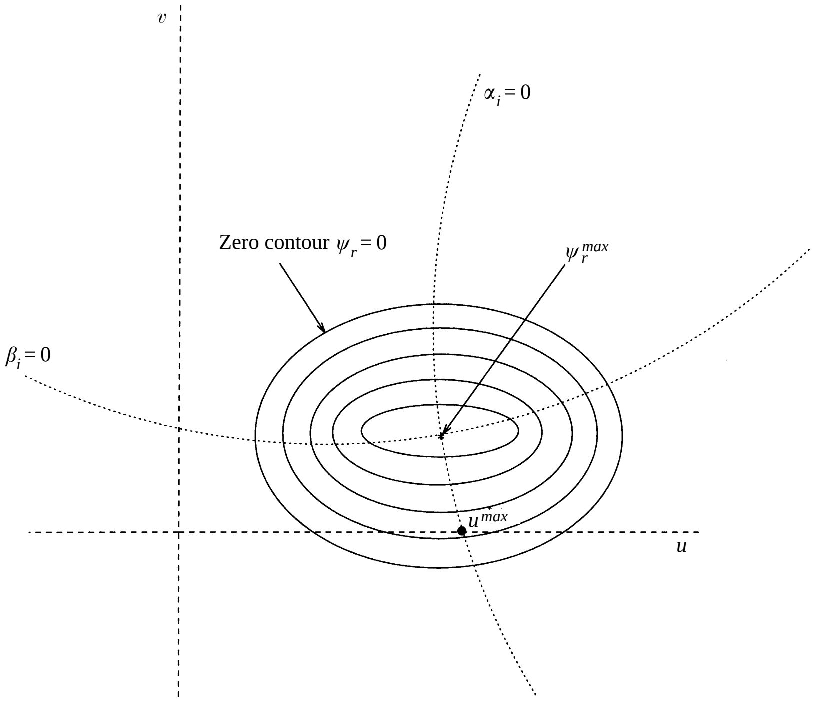

FIGURE 4. Sketch of contours of $\psi_r \geqslant 0$ in the (u, v)-plane.

real axis. We can now use the techniques devised by Briggs (1964) and Bers (1975) for locating an absolute instability in a single-Fourier Green's function to find pinches in the β-plane. We are interested in those pinch points that occur for positive temporal growth rates, i.e. when $\omega_i > 0$. We emphasize again that in order to find an absolute instability in the boundary layer of a swept wing we would require a simultaneous pinch of discrete modes originating in distinct half-planes to occur in the α and β wavenumber planes at a positive value of ω_i (Brevdo 1991) (i.e. simultaneous pinch points in the two wavenumber planes). The group velocity would be zero at such a point, and presumably transition would be triggered in the boundary layer by the growth of disturbances to large amplitudes leading to nonlinearities at a fixed point of space. We were unable to find any such double pinch points. However, as described earlier, significant information about the long-time behaviour of the system can be obtained by considering single pinch points (in the β-plane) for real α, and this will be described in the rest of the paper.

We will refer to mappings of the F-contour at a fixed point on the E-contour into the ω-plane as temporal branches, and the mapping of the L-contour at a fixed point on the E-contour into the β-plane as spatial branches. These mappings are multi-valued, and the Briggs' criterion for a pinch point requires a pinch to occur between two, or more, of the spatial branches, of which at least two must originate from distinct half-β-planes when ω_i is sufficiently large and positive. The crossflow group velocity component $\partial\omega/\partial\beta$ is zero at the pinch point. An entirely equivalent, and for the present problem more convenient, method to locate β pinch points is to study the behaviour of the unstable temporal branches of the mapping of F into the ω-plane. Kupfer, Bers & Ram (1987) demonstrate how the presence of a cusp in the unstable branch in the complex ω-plane is used to locate pinch points and we shall

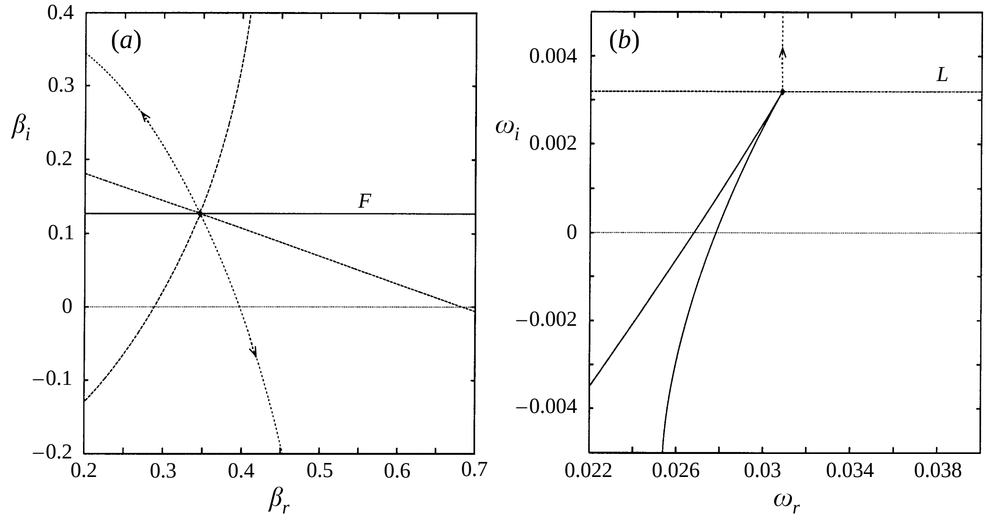

FIGURE 5. A pinch point for $\alpha = 0.1$ and $Re = 1000$. (*a*) The pinch between two spatial branches (dashed-lines) occurring in the β-plane and (*b*) the cusp in the unstable temporal branch in the mapping of F into the ω-plane.

also use this method in our analysis. We now proceed to present results for the model FSC profiles in §3, and for the profiles from a genuine swept airfoil in §4.

3. FSC results

3.1. *Pinch point*

In figure 5 we show the complex ω- and β-planes at a crossflow-induced pinch point for the pressure gradient $\beta_H = 1.0$ and the flow angle $\theta = 45°$, which corresponds to the FSC profile with the crossflow component of largest magnitude, at Reynolds number $Re = 1000$. The value of the streamwise wavenumber, $\alpha = 0.1$, was chosen to correspond to a point close to the maximum positive ω_i for this particular profile. The mapping of the dashed-line contour L in the ω-plane into the β-plane (figure 5*a*) demonstrates the presence of a pinch between two spatial branches in the β-plane. The dotted lines emerging from the pinch point in the β-plane show how the two pinching modes are affected as we increase the value of ω_i from its value at the pinch point (following the arrow in figure 5*b*), and we see how these two lines then extend into distinct halves of the β-plane (indicated by the arrows in figure 5*a*), which is essential for a genuine pinch to occur as described in the previous section. The solid line in the ω-plane graph (figure 5*b*) corresponds to the mapping of the F-contour from the β-plane onto the unstable branch in the ω-plane. Here we can see the presence of a cusp, indicating the presence of a pinch point in the β-plane, and the position of the apex of the cusp corresponds to the value of ω at the pinch point. The group velocity component in this wavenumber direction, $\partial\omega/\partial\beta$, is zero at the pinch point. In this case $\beta_i > 0$, but values of the parameters β_H and θ can also be found for which the pinch occurs in the lower half of the β-plane.

3.2. *Favourable pressure gradient*

In figure 6 we show the range of values of flow angle θ and streamwise wavenumber α for which the unstable pinch points exist, with $\beta_H = 1.0$ and at a range of Reynolds

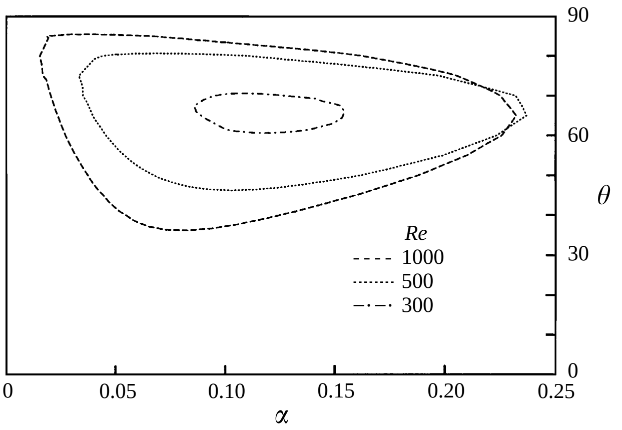

FIGURE 6. Loops of pinch points at $\beta_H = 1.0$ for $Re = 300, 500$ and 1000. The area inside the loops represents regions of unstable pinch points with $\omega_i > 0$ and $\partial\omega/\partial\beta = 0$. The stable region with $\omega_i < 0$ lies outside the loops.

numbers. The regions inside the loops support unstable pinch points in the crossflow direction, while outside the loops $\omega_i < 0$. The size of the region of unstable pinch points increases with increasing Reynolds number, while the minimum flow angle at which a pinch point occurs decreases with increasing the Reynolds number, from 60° at $Re = 300$ to 37° at $Re = 1000$. At $Re = 2000$ (not shown) the minimum flow angle at which a pinch point occurs is 28°. In figure 7 we plot the magnitude of the growth rate at the pinches at a flow angle of $\theta = 65°$, again with $\beta_H = 1.0$, and the destabilizing influence of increasing Reynolds number is clear. For $Re = 280$ the pinch occurs only for negative ω_i and the critical Reynolds number for the onset of an unstable pinch point (i.e. with $\omega_i > 0$) here is approximately 290, and is significantly lower than the critical Reynolds number of 561 for the onset of a chordwise pinch at this value of the pressure gradient found by Lingwood (1997) (the latter was found at a flow angle of $\theta = 82°$). At $\theta = 82°$ and $\beta_H = 1.0$ we find in the present analysis that the critical Reynolds number for an unstable crossflow-induced pinch point is similar to that found by Lingwood for a chordwise pinch point. The parameter values $\beta_H = 1.0$ (representing the flow over a swept wedge of angle 90°) and $\theta = 90°$ (describing a purely spanwise flow) are used to model the flow at the leading edge of a swept wing, and $\theta = 82°$ therefore describes the boundary layer flow at a point very close to the leading edge.

We have therefore found that the minimum critical Reynolds number of 290 for a crossflow-induced pinch occurs at a flow angle of approximately 65° for $\beta_H = 1.0$, while in figure 12 it will be shown that for $\beta_H = 0.5$ a crossflow-induced pinch point mechanism is supported by the boundary layer at a flow angle of 60° and a Reynolds number of 300. It is entirely feasible that the flow over a swept wing may support a boundary layer flow with this flow angle at a pressure gradient close to the value of $\beta_H = 0.5$, and thereby support a pinch point at as low a Reynolds number as 300. (Note that the pressure gradient and flow angle decrease as we proceed down along the chord in the positive-pressure-gradient region of a swept wing.) In figure 2 it is shown that the flow angles $\theta = 70°$ and $\theta = 20°$ have the same crossflow velocity component, but in figure 6 we see that the former flow angle supports an unstable pinch point, while the latter does not. The interaction of the streamwise component

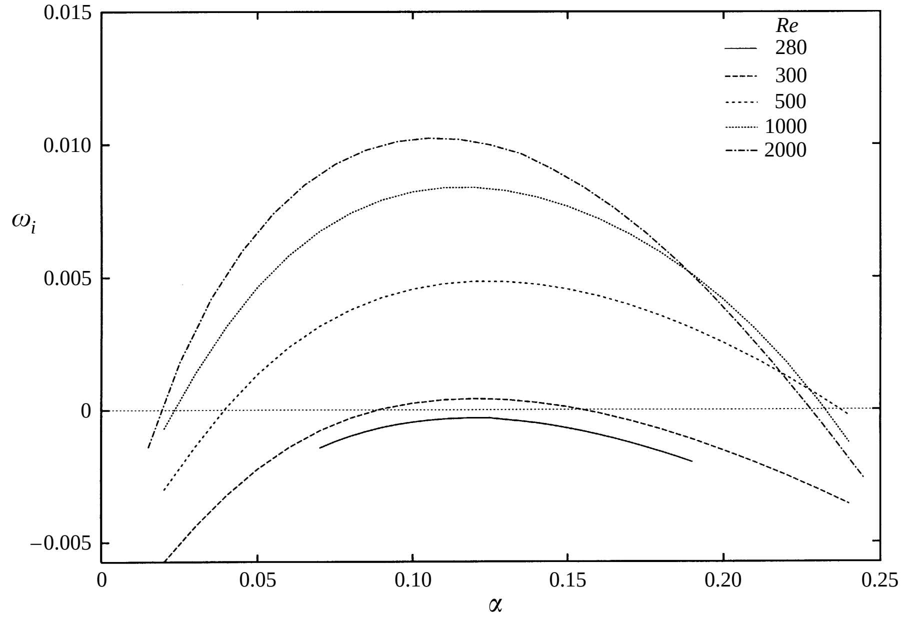

FIGURE 7. Curves of the temporal growth rates at pinch points for $\beta_H = 1.0$ and $\theta = 65°$ at a range of Reynolds numbers, $Re = 280$ to 2000.

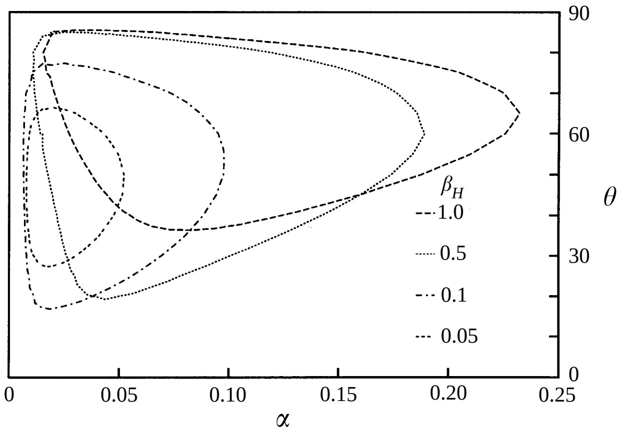

FIGURE 8. Pinch point loops for a Reynolds number of $Re = 1000$ and a range of positive pressure gradients $\beta_H = 0.05$ to 1.0.

of the velocity profile with the crossflow component is therefore important in causing pinch points: a larger streamwise displacement thickness is more unstable.

In figure 8, we show the crossflow-induced pinch point loops for a range of pressure gradients β_H at $Re = 1000$. The range of streamwise wavenumbers and the minimum flow angle at which a pinch point occurs decrease as β_H is reduced from 1.0 to 0.1. In the flow over a swept wing, the flow angle of the streamline on the wing decreases as the pressure gradient is reduced (i.e. at the leading edge the flow is purely spanwise, but as we move down the wing the magnitude of the chordwise component of the velocity increases, thereby reducing the flow angle). In order for a real wing

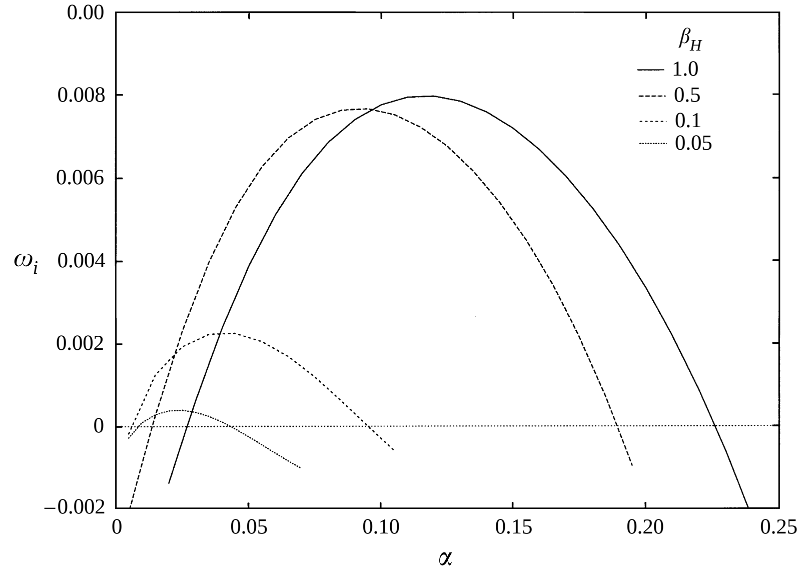

FIGURE 9. Curves of the temporal growth rates at pinch points, at $Re = 1000$ and $\theta = 60^\circ$ for $\beta_H = 0.05$ to 1.0.

to support pinch points we would require the minimum flow angle at which unstable pinch points occur to decrease as the pressure gradient is reduced, and from figure 8 we see that this is indeed the case. As β_H is then decreased from 0.1 to 0.05 in figure 8, the minimum flow angle at which a pinch occurs increases, and this is because, as we saw in figure 2(*a*), the magnitude of the crossflow component of the velocity profiles disappears as β_H tends to zero, so that a crossflow-induced pinch will also disappear in this limit. This effect can also be seen in figure 9, where the magnitude of ω_i at the pinch points at a flow angle of $\theta = 60^\circ$ and a Reynolds number of $Re = 1000$, which is a flow angle close to the largest range of unstable streamwise wavenumbers for each pressure gradient, is shown for the four different pressure gradients used in figure 8. The magnitude of the instabilities decreases dramatically as $\beta_H \to 0$, while the largest value of ω_i changes little between $\beta_H = 1.0$ and $\beta_H = 0.5$.

3.3. *Adverse pressure gradient*

In figure 10 we show the pinch point curves for $\beta_H = -0.1$ at $Re = 1000$ for three flow angles $\theta = 30^\circ$, 45° and 60°. We notice that there is a larger range of streamwise wavenumbers supporting pinch points at the lower flow angle of $\theta = 30^\circ$, while the range and the magnitude of the growth rate at the pinch points has decreased at the higher flow angle of $\theta = 60^\circ$. This is in contrast to the case of positive β_H, where for $\theta < 45^\circ$ the pinch point range and magnitude decrease with decreasing θ, and for $\theta > 45^\circ$ the range and magnitude increase with increasing θ. The pinch points in an adverse pressure gradient flow are more unstable at lower flow angles, and because the flow angle increases from 0° at zero chord length to 90° at infinite chord length in a region of adverse pressure gradient (in contrast to the case of a region of positive pressure gradient where θ goes from 90° at the zero length chord to 0° as the chord length goes towards infinity), the results should be applicable to a genuine swept wing. If we compare figures 9 and 10 we see that the maximum value of ω_i at a pinch point is considerably higher (by a factor of 5) when $\beta_H = -0.1$ than when $\beta_H = 0.1$,

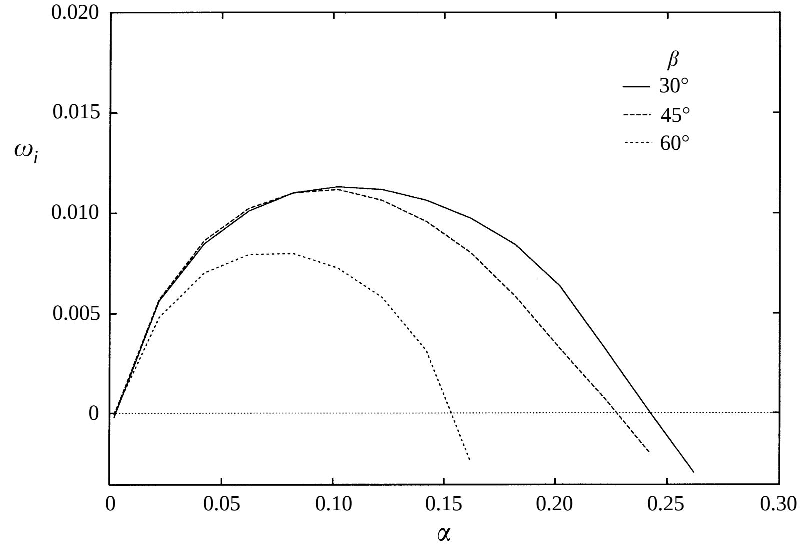

FIGURE 10. Curves of the temporal growth rates at pinch points for a case of negative pressure gradient, $\beta_H = -0.1$, with $Re = 1000$ for three values of the flow angle $\theta = 30°, 45°, 60°$.

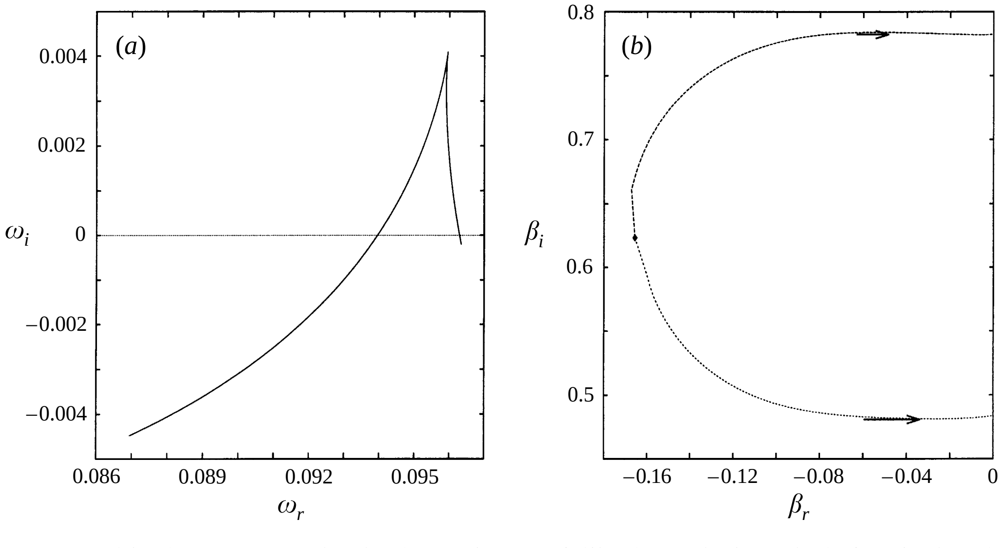

FIGURE 11. (*a*) The cusp occurring in the ω-plane, and (*b*) The equivalent pinch, by plotting the behaviour of the modes as we increase the imaginary part of ω from its value at the pinch point. Both modes remain in the upper half-plane before joining the continuous spectrum along the imaginary β-axis, indicating that this is not a pinch point.

indicating the strong destabilizing influence of a negative pressure gradient. However, despite this larger magnitude the pinch points disappear in the limit of $\beta_H \rightarrow^- 0$, i.e. as the crossflow velocity component disappears. When searching for pinch points at this pressure gradient, we found another region of the parameter space where two modes coalesced in the wavenumber plane in the crossflow direction, an example of which is shown in figure 11. Again we see the characteristic cusp in the ω-plane which has a point of zero crossflow group velocity component, i.e. $\partial\omega/\partial\beta = 0$, at the apex of

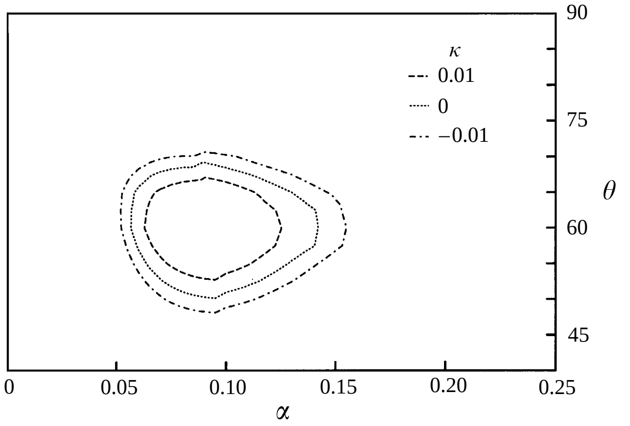

FIGURE 12. Pinch point loops at $\beta_H = 0.5$ and $Re = 300$ for a range of values of the suction/blowing parameter κ.

the cusp. However, when we look at the behaviour of the coalescing modes (indicated by the arrows) in the β-plane as ω_i is increased from its value at the coalescence we see that both modes remain in the upper half-plane. It is a requirement for a pinch point that the modes that coalesce must move into distinct half-planes as we increase the value of ω_i towards infinity, and therefore these coalescing modes are not pinch points. Koch (1986) and Shanthini (1989) discuss how the coalescence of modes that originate in the same half-plane leads to local algebraic growth in Orr–Sommerfeld problems, but we shall not discuss this here.

3.4. *Effect of suction and blowing*

In figure 12 we show the pinch point loops for $\beta_H = 0.5$, corresponding to the flow over a swept wedge of angle 45° and $Re = 300$ with different values of the suction parameter κ. Pinch points are supported at this pressure gradient at a Reynolds number as low as $Re = 300$, which is again significantly lower than the critical Reynolds number, $Re = 561$, for a chordwise pinch point found by Lingwood (1997). The positive value of κ corresponds to an application of wall suction, while the negative value corresponds to blowing and, as we would expect, suction has a stabilizing effect on the pinch points and blowing has a destabilizing effect. Higher levels of suction would remove all pinch points at this Reynolds number for these parameter values. From figure 3 we see that the application of suction corresponds to inward movement of the inflection point and a decrease in the streamwise displacement thickness, and vice versa for blowing. In figure 13 we show the magnitude of the growth rate ω_i at the pinch points for the same value of the pressure gradient at a Reynolds number of 1000, and a flow angle of 60°. In this case we require much higher levels of suction to remove the pinch points, as the magnitudes of ω_i at the pinches are much larger at this higher Reynolds number. Again we see the destabilizing effect of blowing ($\kappa = -0.05$) and the stabilizing effect of suction (positive κ). A level of suction corresponding to the value $\kappa = 0.32$ is required to completely remove the presence of unstable pinch points at these values of the flow parameters.

3.5. *Wave angles*

We define the wave angle, ϕ, to be the angle between the phase fronts of the crossflow-induced pinch points and the streamline, so $\phi = \tan^{-1}(\beta/\alpha)$. In figure 14(*a*)

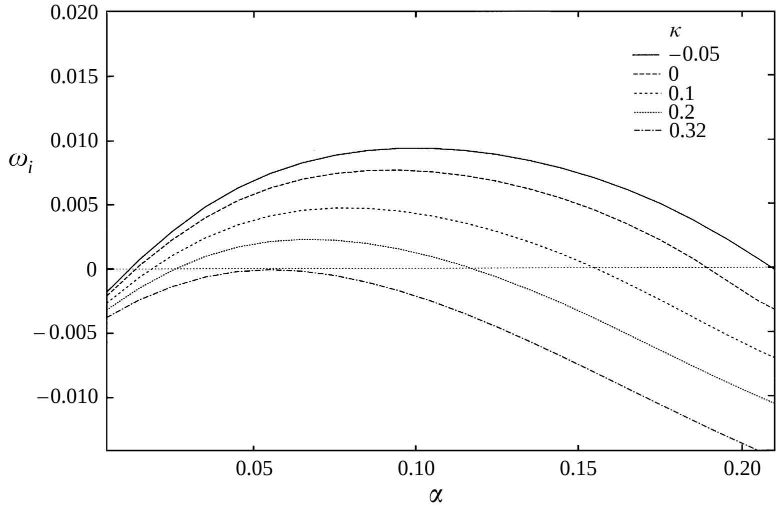

FIGURE 13. Curves of the temporal growth rates at pinch points at $\beta_H = 0.5$, $\theta = 60°$ and $Re = 1000$ for a range of values of the suction/blowing parameter κ.

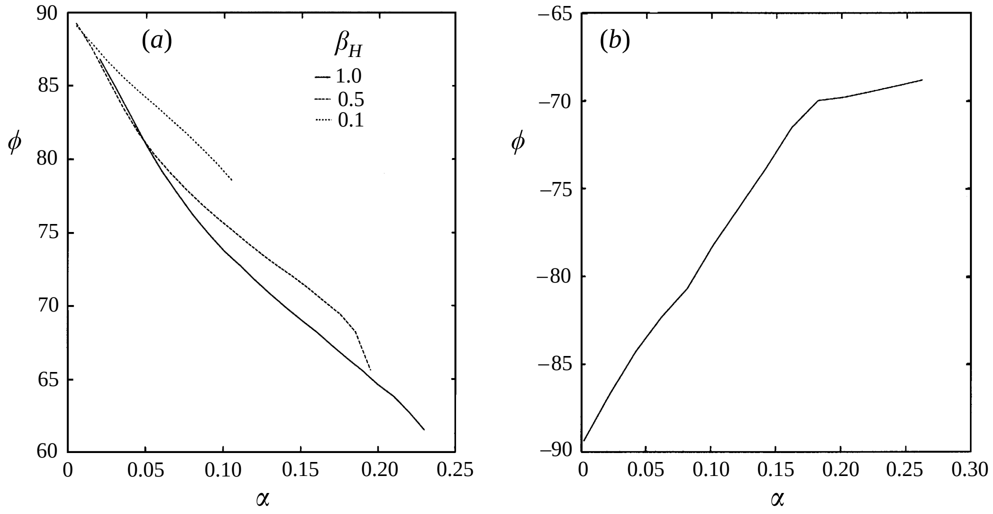

FIGURE 14. Curves of the wave angle ϕ at the pinch points at $Re = 1000$. (*a*) The curves for $\beta_H = 1.0$, 0.5 and 0.1, at a flow angle of 60°. (*b*) The curve for $\beta_H = -0.1$, at a flow angle of 30°.

we see that the wave angles for positive pressure gradient decrease from close to 90° towards 60° as the streamwise wavenumber is increased. (Note that since we are plotting the unstable regions of each curve only, the curve for $\beta_H = 0.1$ is shorter than the others – see figure 8.) We also find that there is little change in the curves as we vary positive β_H, with only a slight increase of wave angle as β_H decreases. Similar results are obtained if we vary the flow angle θ. (The value of $\theta = 60°$ was chosen for the positive-pressure-gradient cases in figure 14(*a*) as it gives a wide range of streamwise wavenumbers, α, with an unstable pinch occurring for each value of β_H.) In figure 14(*b*) we present the same result for the case of negative pressure

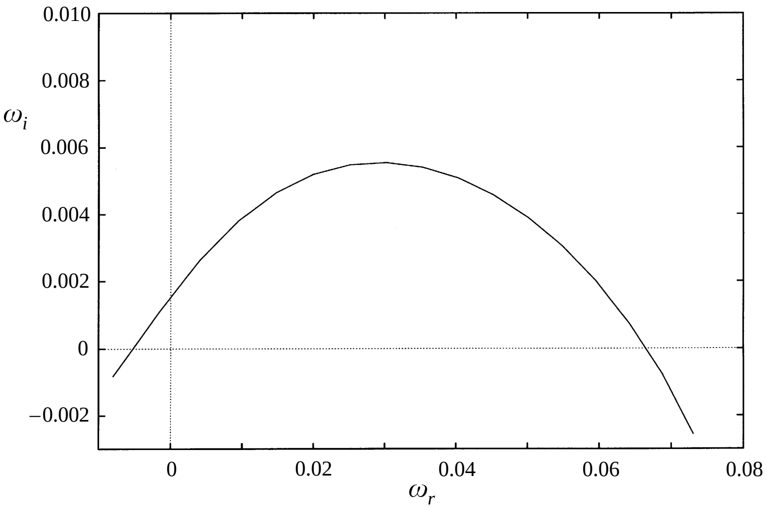

FIGURE 15. The real part of the complex frequency against the imaginary part at the pinch points for the case of $\beta_H = 0.5$, $\theta = 45°$ and $Re = 1000$.

gradient, $\beta_H = -0.1$, but now we choose $\theta = 30°$ to give a wide range of streamwise wavenumbers supporting pinch points for this value of the Hartree parameter. This time the wave angle increases from $-90°$ towards $-70°$ as α increases, so that once again the disturbances are propagating close to the normal of the streamline direction, and are orientated close to the crossflow direction. Note that the sign of the crossflow velocity component changes as β_H changes sign (see figure 2*a*), causing the wave angle of the disturbances to change sign between figures 14(*a*) and 14(*b*). In general ω_r is positive at pinch points, and hence these correspond to travelling disturbances. However, this is not always the case, as we can see from figure 15 where we plot ω_i against ω_r throughout the pinch point region at $\beta_H = 1.0$, $Re = 1000$ and $\theta = 45°$. Here we see that there is an unstable pinch point with a growth rate $\omega_i = 0.0014$ and $\omega_r = 0$ which corresponds to a stationary wave (as the phase velocity has zero real part). Such stationary waves can also be found at other values of the flow parameters.

4. Results for a genuine airfoil

The results in the previous section were calculated for the model FSC boundary layer profiles. Many of the results discussed involved a swept boundary layer flow with strong pressure gradients (i.e. large values of β_H), which are only present in the nose region of a real swept wing. The FSC boundary layers, however, deviate considerably from boundary layers calculated on a genuine wing in the region of rapidly changing pressure gradients which occurs near the leading edge of the wing. Therefore, although the FSC boundary layers have been very useful in investigating the properties of the pinch point mechanism in a qualitative sense for a swept boundary layer, it is necessary to perform an analysis of a genuine swept-wing boundary layer to fully understand the mechanism. It should be noted that non-parallel flow effects might become significant in the region of very large pressure gradient close to the nose, but in this paper we will assume that the flow is locally

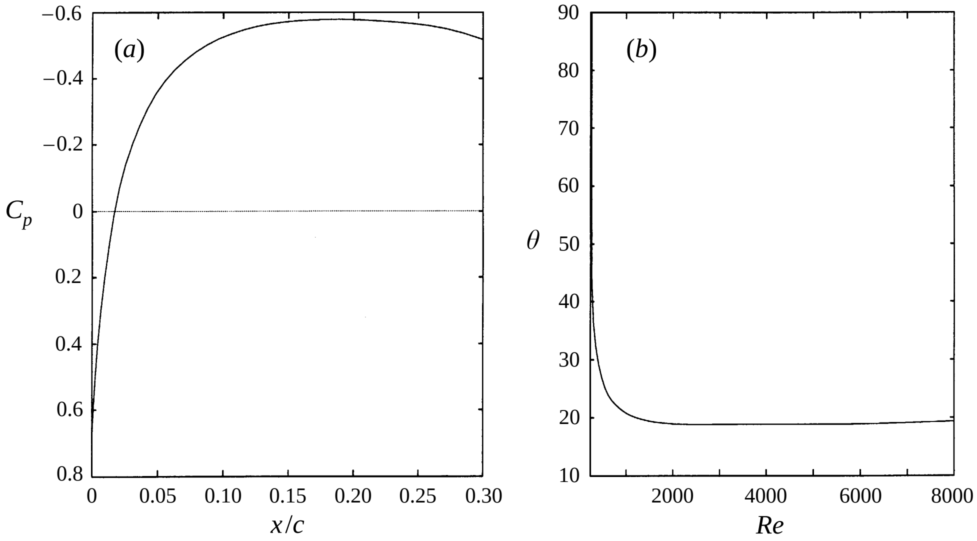

FIGURE 16. (*a*) The pressure coefficient, C_p, curve for the upper surface of the N416 airfoil over the first 30% of chord. (*b*) A plot of Reynolds number based on displacement thickness, *Re*, against flow angle θ. $Re = 255$ at the leading edge, and $Re = 8000$ at 30% of chord.

parallel everywhere. In this section we present results for a genuine swept wing using the NASA natural laminar flow N416 airfoil. The term 'natural laminar flow' refers to an airfoil which is designed to achieve significant regions of laminar flow using favourable pressure gradients only, and this particular airfoil was designed for use on a light single-engined aircraft operating in an incompressible (Mach 0.3/0.4) regime, and it is discussed in Somers (1981). For the purposes of this paper, however, our aim is simply to demonstrate that crossflow-induced pinch points are supported by a physical airfoil.

The airfoil is assumed to be of infinite span and with a sweep angle 25°, chosen to be close to values used for commercial subsonic aircraft. The Reynolds number, R_c, based on chord is 10^7. In figure 16(*a*) we show the pressure coefficient, C_p, over the first 30% of the chord length on the upper surface and the curve is characterized by a strong favourable pressure gradient over the first 10% of chord, followed by a gentle favourable pressure gradient over the next 10% of chord, before entering the adverse pressure region which continues to the rear of the airfoil. In figure 16(*b*) we plot the flow angle θ against Reynolds number *Re* (based on the displacement thickness) over the first 30% of chord and, as discussed previously, θ decreases from a value of 90° at the leading edge as we move in the chordwise direction, followed by a very gradual increase in θ as we enter the region of adverse pressure gradient. Using exactly the same approach as described in the previous section, crossflow-induced pinch points were again found. In figure 17 we plot the growth rate ω_i maximized over real α at a pinch point (which gives the maximum growth rate in the streamwise direction) over the first 12% of chord. Initially there is a large increase in the growth rate as we enter the unstable region and the Reynolds number *Re* increases, but this is followed by a gentle decrease in the growth rate, because the reduction in the favourable pressure gradient as we proceed down the wing chord has a stabilizing effect on the boundary layer (see figure 9). This effect is partially balanced by the destabilizing influence of increasing *Re* as we move down the wing chord. In figure 18 we plot ω_r against the

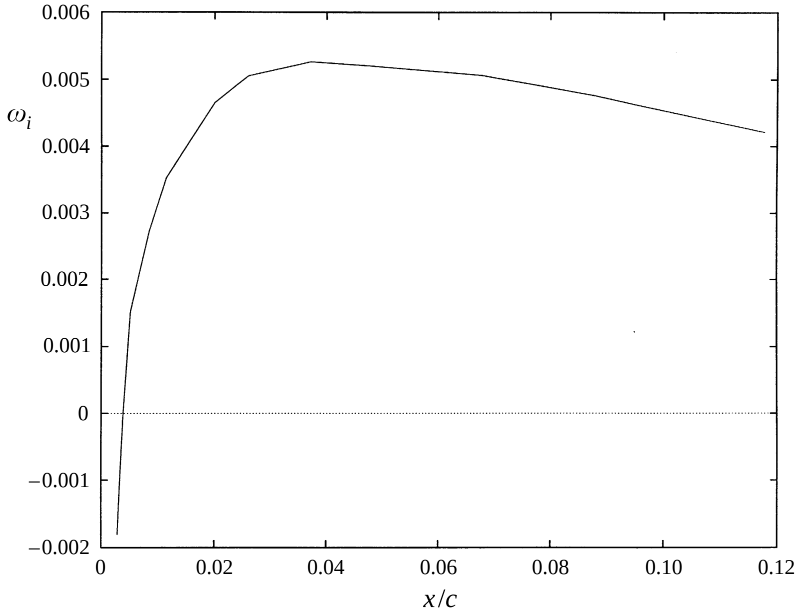

FIGURE 17. Plot of maximum growth rate ω_i at a pinch against percentage chord, x/c, for the N416 airfoil at 25° sweep with $R_c = 10^7$.

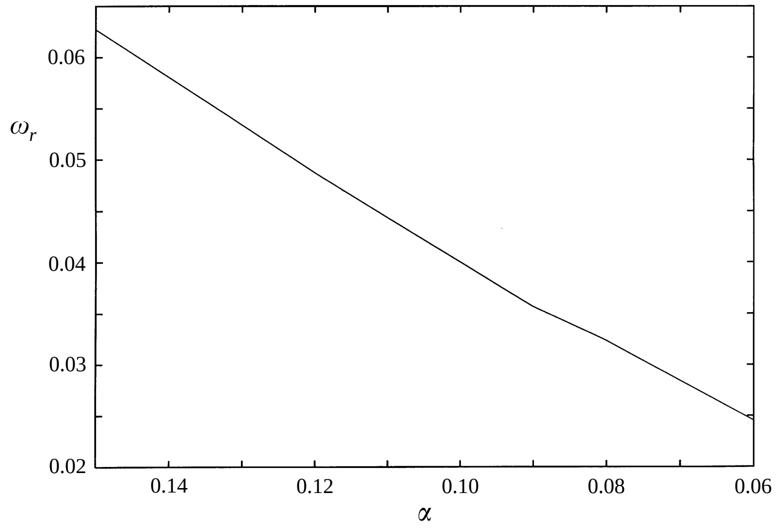

FIGURE 18. Real streamwise wavenumber α against real part of complex frequency ω_r at maximum growth rate at a pinch ω_i over the first 10% of chord for the N416. At 10% chord the values of α and ω_r at the maximium value of ω_i are 0.06 and 0.025 respectively.

streamwise wavenumber α at the maximum growth rate ω_i, over the unstable region of the first 12% of chord and the value of ω_r and α at the maximum value of the growth rate ω_i is seen to decrease as we move down the airfoil, i.e. as the pressure gradient decreases.

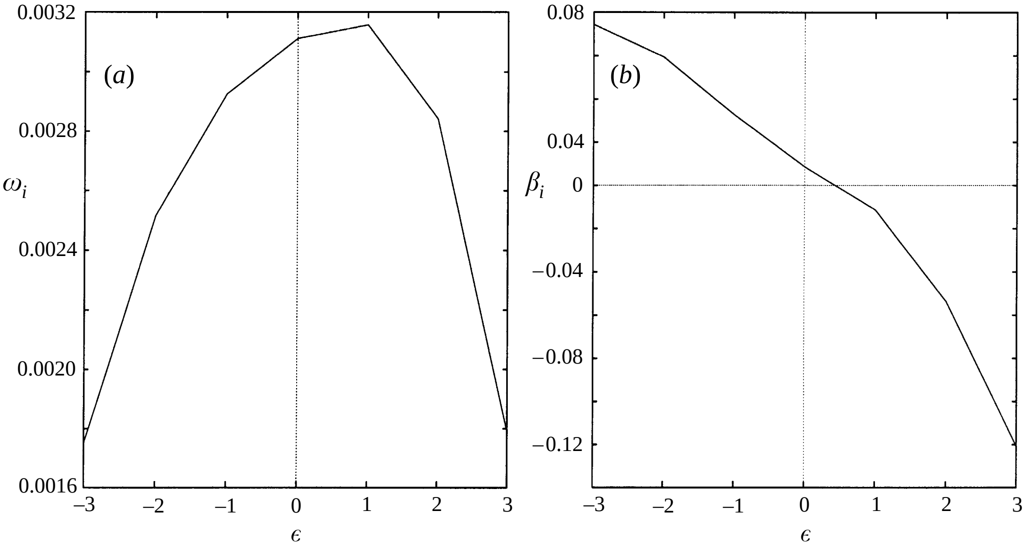

FIGURE 19. (*a*) The maximum temporal growth rate ω_i in the directions $\epsilon = -3°, -2°, -1°, 0°, 1°, 2°, 3°$. (*b*) The value of β_i at these pinch point.

5. Variation of search direction

The analysis in the previous two sections has been concerned with locating pinch points in the crossflow transform plane, and thereby calculating the maximum temporal growth rate contained in wavepackets propagating in the streamwise direction (i.e. $v = 0$). However, this technique can be used to determine the maximum growth for propagation in any given direction (i.e. arbitrary values of the ratio $v/u \equiv \tan\epsilon$), and in particular to find ψ_r^{max}, the maximum possible growth rate in the (u, v)-plane (see figure 4). In order to do this we resolve the streamwise and crossflow velocity profiles as

$$U'(\eta) = U(\eta)\cos\epsilon - W(\eta)\sin\epsilon,$$

$$W'(\eta) = U(\eta)\sin\epsilon + W(\eta)\cos\epsilon,$$

and search for pinch points in the new wavenumber plane corresponding to the direction of the W' component of the velocity profile. In figure 19(*a*) we show the maximum growth rates for a range of values of ϵ for the case of the FSC profile with $\beta_H = 0.5$, $Re = 400$ and $\theta = 60°$; the maximum value occurs for $\epsilon = 1.0°$. In figure 19(*b*) we plot the value of the imaginary part of the wavenumber in the direction of the W' component of the velocity at the pinch points of maximum growth for each value of ϵ, and see that $\beta_i = 0$ when $\epsilon = 0.8°$. In figure 4 it is shown that the point of maximum growth rate in the (u, v)-plane, ψ_r^{max}, is located at the intersection of the $\alpha_i = 0$ and $\beta_i = 0$ curves, and by rotating the axes through $\epsilon = 0.8°$ in this case we have mapped the u-axis onto this point. It is interesting to note that the maximum growth rate in any given direction, i.e. the maximum growth rate of the travelling wave system, is purely temporal in nature, as both wavenumbers are real.

In figure 20 we plot the values of the imaginary part of the crossflow wavenumber β_i for the N416 airfoil at the points of maximum growth rate plotted in figure 17. The value of β_i decreases quickly away from the leading edge, before a more gentle reduction further down the wing. Between 4% of chord and 12% of chord the value

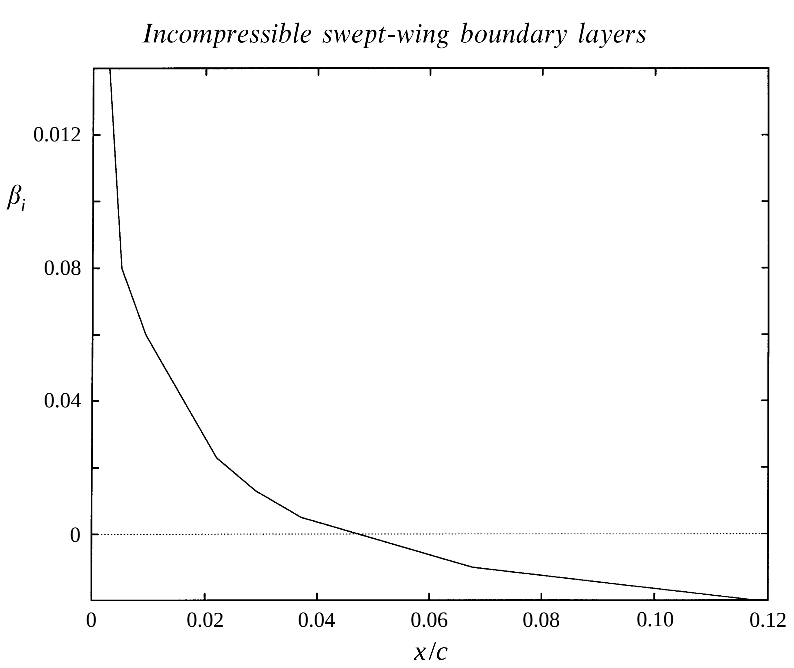

FIGURE 20. β_i at the pinch points in the streamwise direction of maximum temporal growth rate ω_i over the first 12% chord of the N416.

of β_i is quite close to zero, indicating that the maximum value of ψ_r occurs in a direction close to the streamwise direction, i.e. a small value of ϵ will locate the direction of maximum growth rate. However, nearer the leading edge β_i is much larger, and we would have to use a large value of ϵ in order to resolve the profiles into the direction of maximum amplification. Lingwood (1997) has shown that the swept-wing boundary layer supports pinch points in the chordwise direction in the region close to the leading edge of the leading edge, and therefore in order to locate the direction of maximum amplification close to the leading edge of the wing we have to resolve our velocity profiles in a direction away from the streamwise/crossflow direction and towards the chordwise/spanwise direction.

6. Conclusions

In this paper we have analysed the behaviour of pinch points in the wavenumber plane corresponding to the crossflow direction, and have described the effects of variation in pressure gradient, flow angle and suction levels using linear stability theory for the FSC boundary layer. It was then demonstrated that these pinch points are supported in the boundary layer of a genuine swept wing. We have shown how the pinch points can be used to find the maximum temporal growth rate obtained by a single wave contained in the wavepacket in a given direction and, by searching for the direction that gives the maximum growth rate, how the maximum local amplification rate of the travelling wave system can be determined. Brevdo (1991) has suggested a scheme for computing N-factors for an e^N transition prediction scheme by integrating the maximum local growth rates obtained by a single wave contained in the convectively unstable wavepackets along the wing, where

$$N = \int_\gamma \frac{\omega_i}{V_g(s)} \mathrm{d}s,$$

and the path γ is the integral curve in the direction of the group velocity vector V_g of the maximal temporal growth rate. We suggest that by using the pinch point property of the swept-wing boundary layer to locate the maximum amplification rate at each point on the γ-curve, and integrating these growth rates to calculate an N-factor, we can measure the amplification contained in convective wavepackets on the swept-wing boundary layer. Such an approach would have the advantage of describing the evolution of the maximum amplified wave for varying frequencies contained in wavepackets at each chordwise station, rather than just modes of a single frequency only, as used in a conventional e^N analysis. It would also be possible to study the behaviour of all the unstable waves contained in the wavepacket in this way. Oertel & Delfs (1995) used the saddle point criterion (equations (9) and (10)) to examine the behaviour of the convective wavepacket generated by an impulse for two chordwise stations on a swept wing. However, modifications in the growth of the wavepacket caused by the changes that occur in the boundary layer of the swept wing downstream of the impulse were not taken into account. This is also a weakness of Brevdo's scheme. However, the location of the maximum amplification of a single wave using the pinch point property at each chordwise station provides a measure of the total amplification contained in the convecting wavepackets, which we suggest is a useful quantity for use in an e^N-type transition prediction technique. These ideas will be described in detail in a future paper, where we shall also extend the analysis into the high-speed compressible regime for application to commercial aircraft.

The authors are grateful to Dr F. Lam for calculating the boundary layer profiles in §4. M.J.T. acknowledges the support of EPSRC and British Aerospace Airbus Ltd in the form of a CASE studentship. The authors would also like to thank Professor M. Gaster and Dr R. Lingwood for many useful discussions.

REFERENCES

Bers, A. 1975 Linear waves and instabilities. In *Physique des Plasmas* (ed. C. DeWitt & J. Peyraud), pp. 113–215. Gordon and Breach.

Betchov, R. & Criminale, W. 1966 Spatial instability of the inviscid jet and wake. *Phys. Fluids* **9**, 359–362.

Brazier-Smith, P. & Scott, J. 1984 Stability of fluid flow in the presence of a compliant surface. *Wave Motion* **6**, 547–560.

Brevdo, L. 1991 Three-dimensional absolute and convective instabilities, and spatially amplifying waves in parallel shear flows. *Z. Angew. Math. Phys.* **42**, 911–942.

Briggs, R. 1964 *Electron-Steam Interaction with Plasmas.* MIT Press.

Cooke, J. 1950 The boundary layer of a class of infinite yawed cylinders. *Proc. Camb. Phil. Soc.* **46**, 645–648.

Gray, W. 1952 The nature of the boundary layer at the nose of a swept back wing. *Unpublished, Min. Aviation, Lond.*

Gregory, N., Stuart, J. & Walker, W. 1955 On the stability of three-dimensional boundary layers with application to the flow due to a rotating disk. *Phil. Trans. R. Soc. Lond.* A **248**, 155–199.

Hall, P., Malik, M. & Poll, D. 1984 On the stability of the infinite swept attachment line boundary layer. *Proc. R. Soc. Lond.* A **395**, 229–245.

Huerre, P. & Monkewitz, P. 1985 Absolute and convective instabilities in free shear layers. *J. Fluid Mech.* **159**, 151–168.

Koch, W. 1985 Local instability characteristics and frequency determination of self-excited wake flows. *J. Sound Vib.* **99**, 53–83.

Koch, W. 1986 Direct resonance in Orr–Sommerfeld problems. *Acta Mechanica* **58**, 11–29.

Kupfer, K., Bers, A. & Ram, A. 1987 The cusp map in the complex-frequency plane for absolute instabilities. *Phys. Fluids* **30**, 3075–3082.

Lingwood, R. 1995 Absolute instability of the boundary layer on a rotating disk. *J. Fluid Mech.* **299**, 17–33.

Lingwood, R. 1996 An experimental study of absolute instability of rotating-disk boundary-layer flow. *J. Fluid Mech.* **314**, 373–405.

Lingwood, R. 1997 On the impulse response for swept boundary layer flows. *J. Fluid Mech.* **344**, 317–344.

Mack, L. 1984 Special course on stability and transition of laminar flow. *AGARD Rep.* 709, NATO.

Malik, M. 1990 Numerical methods for hypersonic boundary layer stability. *Comput. Phys.* **86**, 376–413.

Malik, M. & Orszag, S. 1980 Comparison of methods for prediction of transition by stability analysis. *AIAA J.* **18**, 1485–1489.

Malik, M., Li, F. & Chang, C. 1994 Crossflow disturbance in three-dimensional boundary layers: nonlinear development, wave interaction and secondary instability. *J. Fluid Mech.* **268**, 1–36.

Oertel, H. & Delfs, J. 1995 Mathematische analyse der bereiche reibungsbehafteter stromungen. *Z. Angew. Math. Mech.* **75**, 491–505.

Poll, D. 1985 Some observations of the transition process on the windward face of a long yawed cylinder. *J. Fluid Mech.* **150**, 329–356.

Rosenhead, L. 1963 *Laminar Boundary Layers.* Oxford University Press.

Shanthini, R. 1989 Degeneracies of the temporal Orr–Sommerfeld eigenmodes in plane poiseuille flow. *J. Fluid Mech.* **201**, 13–34.

Somers, D. 1981 Design and experimental results for a natural-laminar flow airfoil for general aviation applications. *Tech. Paper* 1861. NASA.

Taylor, M. J. 1997 The stability of the boundary layer on swept wings. PhD thesis, University of Cambridge.

Van Ingen, J. 1956 A suggested semi-empirical method for the calculation of the boundary layer transition region. *Rep.* VTH-74, University of Technology Delft.